ACS OMEGA

http://pubs.acs.org/journal/acsodf

Article

Upconversion Luminescence via Anion Exchange in Perovskite Quantum Dots for Anticounterfeiting Inkjet Printing

Xiang Zheng,* Yuan Wen, Jun Zhong, and Ai-Zheng Chen*

Cite This: *ACS Omega* 2022, 7, 40596−40602

Read Online

ACCESS | Metrics & More | Article Recommendations | Supporting Information

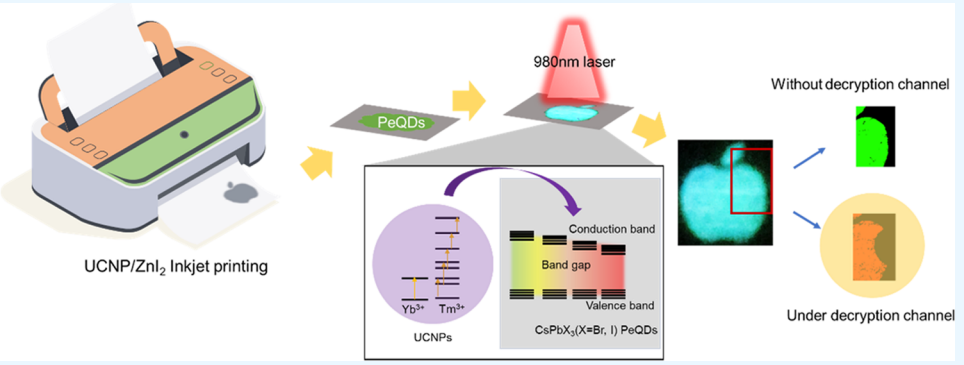

ABSTRACT: Lanthanide-doped upconversion nanoparticles (UCNPs) and cesium lead halide perovskite quantum dots (PeQDs) are highly compatible with each other: UCNPs produce anti-Stokes upconversion luminescence (UCL) under near-infrared (NIR) excitation and the emissive profiles of PeQDs can be conveniently tuned by varying the halide composition ratio. Therefore, in this study, UCNPs and PeQDs are mixed together, producing colorful UCL under 980 nm laser excitation. In addition, ZnI_2 is used to vary the halide composition ratio of PeQDs and manipulate UCL in situ, thus adding more flexibility in UCL regulation. Finally, based on the above-mentioned discussion, a double-encrypted anticounterfeiting pattern is generated via sequentially printing ZnI_2 solution and UCNP suspension on an A4 paper. Using PeQDs as the decrypting reagent, under the NIR excitation and decryption channel, the hidden information can be fully decrypted. The combination of UCNPs and PeQDs greatly expands the upconversion possibility, offers more feasibility in UCL regulation, and further promotes the practical applications.

1. INTRODUCTION

In the past decade, cesium lead halide (CPX_3, X = Cl, Br, and I) perovskite quantum dots (PeQDs) have attracted a lot of attention due to the outstanding optical properties such as the large absorption coefficient, high quantum yields, emission peaks with narrow full width at half maximum (FWHM), and so on.[1,2] In addition, the ease of tuning the band gap via modulating the halide composition, thus shifting the single-peak emissive profiles from deep blue to red continuously, endows the materials with huge potential in wide applications such as displays, photovoltaics, optoelectronics, and so on.[3−8] Meanwhile, lanthanide-doped upconversion nanoparticles (UCNPs), giving off anti-Stokes upconversion luminescence (UCL) under 980 nm NIR laser excitation, have demonstrated unparallel virtues against Stokes luminescence in various fields.[9−13] However, unlike PeQDs, UCNPs critically rely on the dopants' energy levels, with fixed UCL emissive peaks at certain wavelengths. Consequently, the UCL manipulation strategy has always been intensively focused over the decades. Notably, Tm^{3+}-doped UCNPs can produce efficient UV (345, 356 nm) and blue (450, 475 nm) emissions under 980 nm NIR excitation, which lie in the ideal excitation wavelength ranges of PeQDs.[14] Therefore, should UCNPs and PeQDs be coupled together, colorful UCL could be expected from the UCNP−PeQD pairs. There are quite a few articles featuring the coupling between UCNPs and PeQDs, e.g., Ruan et al. reported the synthesis of heterostructured upconversion perovskite nanoparticles, where PeQDs and UCNPs are merged together, generating a new nanocomposite;[15] Wei et al. reported using UCNP and PeQD mixtures to generate UCL with different single-peak emission profiles;[16] and Du et al. linked PeQDs on the surface of UCNPs via the seed growth strategy.[17] UCNP and PeQD pairs have also demonstrated the application potential in various fields, such as photovoltaics, optics, patterning, and so on.[18−20] However, using halide composition tuning strategy to vary UCL after UCNPs and

Received: October 7, 2022
Accepted: October 14, 2022
Published: October 25, 2022

PeQDs are coupled together, i.e., in situ UCL manipulation, has never been explored before. Therefore, in this study, we focus on modulating the UCL via PeQDs and tuning the UCL using ZnI_2; this in situ UCL tuning strategy is are further used to generate anticounterfeiting patterns with double-encrypted information that can only be extracted under the NIR excitation wavelength and decryption channel.

To begin with, $NaYF_4$:30%Yb,0.5%Tm@$NaYF_4$ UCNPs and cesium lead halide PeQDs with different halide compositions are synthesized and characterized. Next, coupling between UCNPs and PeQDs is studied, different UCNP−PeQD pairs exhibit colorful UCL under 980 nm laser illumination. Subsequently, ZnI_2 is used to manipulate the UCL, and emissive profiles are red-shifted with increasing ZnI_2 addition amount. Finally, based on the UCL manipulation strategy mentioned above, double-encrypted anticounterfeiting patterns are generated via sequentially printing UCNPs and ZnI_2 solution into the designed region: by brushing a thin layer of PeQDs on top, under 980 nm laser illumination, the encrypted information could be extracted only under the right decryption channel.

2. EXPERIMENTAL SECTION

2.1. Chemicals. $YbCl_3·6H_2O$ (Adamas, 99%), $TmCl_3·6H_2O$ (Adamas, 99%), $YCl_3·6H_2O$ (Adamas, 99%), Cs_2CO_3 (Adamas, 99.99%), $PbCl_2$ (Adamas, >99%), $PbBr_2$ (Adamas, 99.999%), PbI_2 (Adamas, >99%), oleic acid (OA, 90%, Sigma-Aldrich), 1-octadecene (ODE, 90%, Sigma-Aldrich), oleylamine (OAm, 98%, Sigma-Aldrich), cyclohexane (98%, Sigma-Aldrich), methanol (Sinopharm, 99.9%), NaOH (Sinopharm, 98%), NH_4F (Aladdin, 98%), and toluene (98%, Sigma-Aldrich) are used. All chemicals are used as received without further purification.

2.2. Synthesis of β-Phase $NaYF_4$:30%Yb,0.5%Tm Core Nanocrystals. $NaYF_4$:30%Yb,0.5%Tm nanocrystals are synthesized using a well-developed high-temperature coprecipitation method previously reported by our group.[21] Typically, based on the composition, a total amount of 1 mmol $RECl_3$ (RE = Y, Yb, Tm) aqueous solution is added into a 100 mL flask stoichiometrically. After water is fully evaporated, 15 mL of 1-octadecene and 6 mL of oleic acid are added; the mixture is reacted at 156 °C for 10 min to form RE-oleate complexes. The resulting solution is cooled to room temperature and then mixed with a methanol solution (5 mL) containing NH_4F (4 mmol) and NaOH (2.5 mmol). After that, the temperature is increased to 120 °C for 10 min for complete methanol removal. Then, the solution is degassed for 15 min to remove residual methanol and oxygen. Subsequently, the resulting solution temperature is increased to 300 °C for 1 h under an inert gas environment. The products are precipitated with acetone, centrifuged at 6000 rpm for 10 min, washed with acetone, dispersed in 10 mL of cyclohexane, and stored for further use.

2.3. Synthesis of $NaYF_4$:30%Yb,0.5%Tm@$NaYF_4$ Core−Shell Nanocrystals. Core−shell UCNPs are prepared via the epitaxial growth method previously reported by our group.[21] The as-prepared core nanoparticles of $NaYF_4$:30% Yb,0.5%Tm are used as seeds for inert shell growth. In a typical process, an aqueous solution of YCl_3 (1 mL, 1 mmol) is added into a 100 mL flask; after water is fully evaporated, 15 mL of 1-octadecene and 6 mL of oleic acid are added. The mixture is kept at 156 °C for 10 min to form Lu-oleate complexes. Upon cooling of the Y-oleate precursors to room temperature, the as-prepared core nanoparticles are added, and the resulting mixture is then heated at 120 °C for 20 min to fully evaporate the cyclohexane. Subsequently, the reaction solution is cooled to room temperature, followed by the addition of a methanol solution (5 mL) containing NH_4F (4 mmol) and NaOH (2.5 mmol). The resulting mixture is vigorously stirred and then heated at 120 °C for 10 min. After that, the reaction mixture is degassed for 10 min to evaporate the residual methanol and oxygen in the solution. Finally, the temperature is increased to 300 °C, and the mixture is kept under an argon atmosphere for 1.5 h. The resultant nanoparticles are precipitated after the addition of acetone under 8000 rpm centrifugation for 10 min, washed with acetone, and finally dispersed in 20 mL of cyclohexane for further usage.

2.4. Synthesis of PeQDs Via a Hot Injection Method. CPX_3 (X = Cl, Br, and I) PeQDs are prepared through a modified hot injection method using Cs_2CO_3 as the Cs^+ source. In typical synthesis procedures, 814 mg of Cs_2CO_3 powder is mixed with 40 mL of ODE and 2.5 mL of OA into a tri-neck round-bottom flask. With vigorous stirring, the mixture is heated to 120 °C under vacuum. After the transparent Cs-oleate solution is formed, the reaction flask is maintained at 120 °C under vacuum for another 10 min to fully evaporate the water. The mixture is heated to and maintained at 150 °C under an argon atmosphere to prepare for the hot injection. On the other hand, 1 mmol PbX_2 (X = Br, I) salts are mixed with 30 mL of ODE, 3 mL of OA, and 2.5 mL of OAm. With vigorous stirring, the mixture is heated to 120 °C under vacuum. After the transparent solution is formed, the reaction flask is maintained at 120 °C under vacuum for 10 min to fully evaporate the water. The mixture is then heated to and maintained at 150 °C under an argon atmosphere to prepare for the injection.

After the two reaction vessels reached and were stabilized at 150 °C, 2.4 mL of Cs-oleate solution is withdrawn from the first tri-neck flask and quickly injected into the second PbX_2 flask. After 10 s, the reaction vessel is taken out from the heating mantel and quickly cooled to room temperature via an ice bath. The resulting mixture is centrifuged and redispersed in cyclohexane and then sealed for further use.

2.5. Ligand-Free UCNP Preparation. Ligand-free UCNPs are prepared by a ligand exchange method. Briefly, 0.1 M HCl solution is prepared by adding hydrochloric acid into water. Subsequently, 2 mL of UCNP cyclohexane solution is mixed with an equal amount of HCl solution. Then, the mixture is vigorously stirred and vortexed for 45 min, forming a white turbid mixture. The mixture is stood still for 5 min to separate it into two immiscible layers before pipetting out the top layer. Note that after the ligand exchange is completed, the top layer should not exhibit UCL under a NIR laser. The above-prepared ligand-free UCNPs are washed and purified using water and ethanol thrice to fully remove the HCl. The washed ligand-free UCNPs are dispersed in water and kept for further use.

2.6. Ink Preparation and Pattern Printing. A 1% weight in volume Pluronic F-127 water solution is prepared first. A total of 10 μL of the as-prepared F-127 solution is added to every 1 mL ligand-free UCNP water suspension. A total of 3 mL of the as-prepared UCNPs is added into an empty printer cartridge of a Canon MG3100 followed by normal printing steps.

A total of 200 mg of ZnI_2 is dissolved in 10 mL of water followed by vigorous stirring to form a homogeneous solution.

https://doi.org/10.1021/acsomega.2c06464
ACS Omega 2022, 7, 40596−40602

Scheme 1. Schematic Illustration of (a) PeQD and (b) UCNP Synthesis Routes

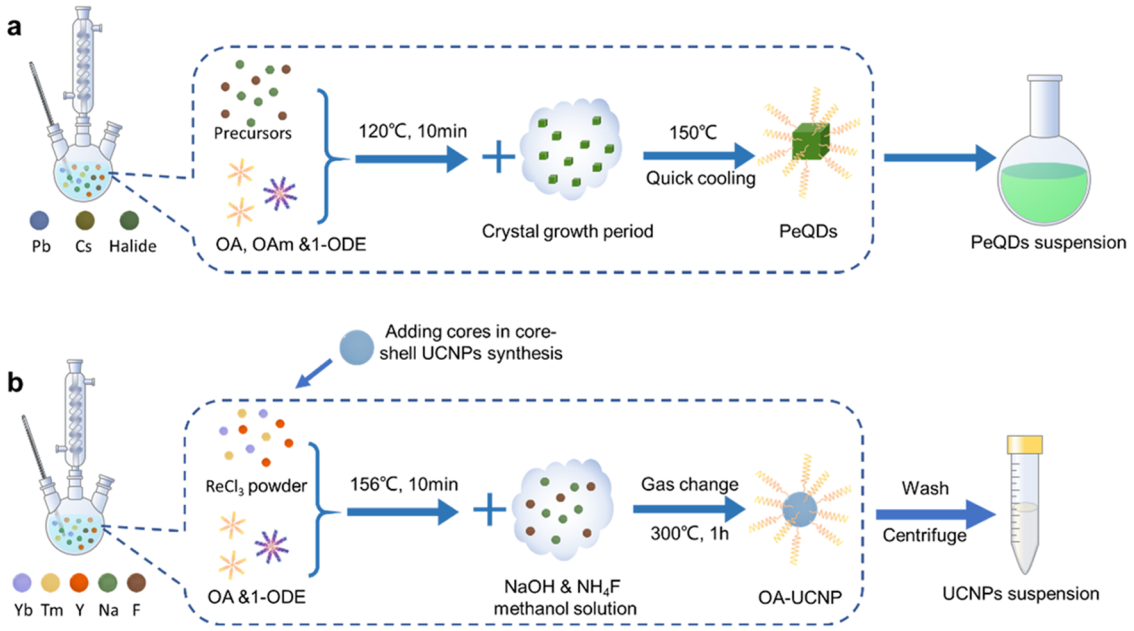

A total of 3 mL of ZnI_2 solution is added into an empty printer cartridge of a Canon MG3100 followed by normal printing steps.

2.7. Physical Characterization. Transmission electron microscopy (TEM) images of UCNPs are recorded on a JEOL 2010F transmission electron microscope (Jeol Ltd., Tokyo, Japan) operating at an acceleration voltage of 200 kV. Luminescence spectra of UCNPs are recorded on a Hitachi F-500 fluorescence spectrophotometer (Hitachi High-Technologies Corporation, Tokyo, Japan) equipped with a NIR continuous-wave (CW) laser with emission at 980 nm (Photonitech (Asia) Pte. Ltd., Singapore). Optical decryption is performed under a μFluor-980 small-animal upconversion luminescence imaging system (Einst Technology Pte Ltd., Singapore).

3. RESULTS AND DISCUSSION

3.1. Material Synthesis and Characterization. The study begins with the synthesis of UCNPs and PeQDs (Scheme 1). PeQDs are synthesized based on an adapted protocol. Details and abbreviations of the PeQD samples used in the study are summarized in Table 1. Under TEM, uniformly distributed PeQDs can be observed with a cubic shape and 10 nm in size (Figure 1a–d). XRD characterization reveals that the PeQDs are well crystalized with a cubic crystal phase (Figure S1). Under UV excitation, colorful luminescence can be captured using a camera (Figure 1e). Based on the UV–Vis absorption data, all PeQD samples exhibit a strong absorption band in UV and blue ranges (Figure 1f). Emission spectra of different PeQDs are obtained under 365 nm UV excitation; all of the PeQD suspensions give off intense single-peak emissive profiles; the emission peaks of PeQDs are gradually red-shifted as an increasing amount of the bromide ions within PeQD crystals is substituted by iodine ions (Figure 1g).

Table 1. Abbreviations and Compositions of the PeQD Samples Used in the Study

name	composition	Cl/Br/I
CPX510	$CsPbBr_3$	0:3:0
CPX540	$CsPb(Br/I)_3$	0:2:1
CPX610	$CsPb(Br/I)_3$	0:1:2
CPX650	$CsPb(Br/I)_3$	0:0.75:2.25

Since PeQDs can be effectively activated by UV/blue light, Tm-doped UCNPs with excellent UV and blue upconversion emissive peaks are selected and synthesized in our study. To improve the UV/blue emissive intensity, an inert protective $NaYF_4$ shell layer is epitaxially grown on the core. From TEM images, it is observed that core and core–shell UCNPs have uniformly distributed size and morphology (Figure 2a,b). Core UCNPs are spherical in shape, with the diameter focused at 40 nm, while core–shell UCNPs exhibit an elongated spherical shape, with 60 nm length and 50 nm width. XRD reveals that the UCNPs are well crystalized with a hexagonal phase (Figure S2). Under 980 nm excitation, strong UV and blue UCL can be detected using both spectrometer and CCD camera: compared with cores, core–shell UCNPs exhibit much stronger UCL, as the well-protected surface greatly reduces the surface quenching effect (Figure 2c,d). The as-prepared $NaYF_4$:30%Yb,0.5%Tm@$NaYF_4$ core–shell UCNPs are stored and used in the following experiments.

3.2. Coupling between UCNPs and PeQDs. After UCNPs and PeQDs are successfully prepared, we move on to exploring the coupling between PeQDs and UCNPs and using PeQDs to modulate UCL. The experiments start with CPX510. A total of 100 μL of UCNPs is mixed with increasing amount of CPX510 from 0 to 300 μL, with the overall volume kept the same at 1 mL throughout the experiments. Based on the spectra, it is obvious that the emissions from UCNPs are gradually absorbed by CPX510 and disappeared with increasing amount of PeQDs added; at the same time, emissions from PeQDs increased quickly and took over the overall emissive profile, generating a single emission peak (Figure 3a). Camera photos also support our findings as the color of the overall suspension shifted from purple (UCNPs' intrinsic color) to green (Figure 3b,c). The coupling study is

https://doi.org/10.1021/acsomega.2c06464
ACS Omega 2022, 7, 40596–40602

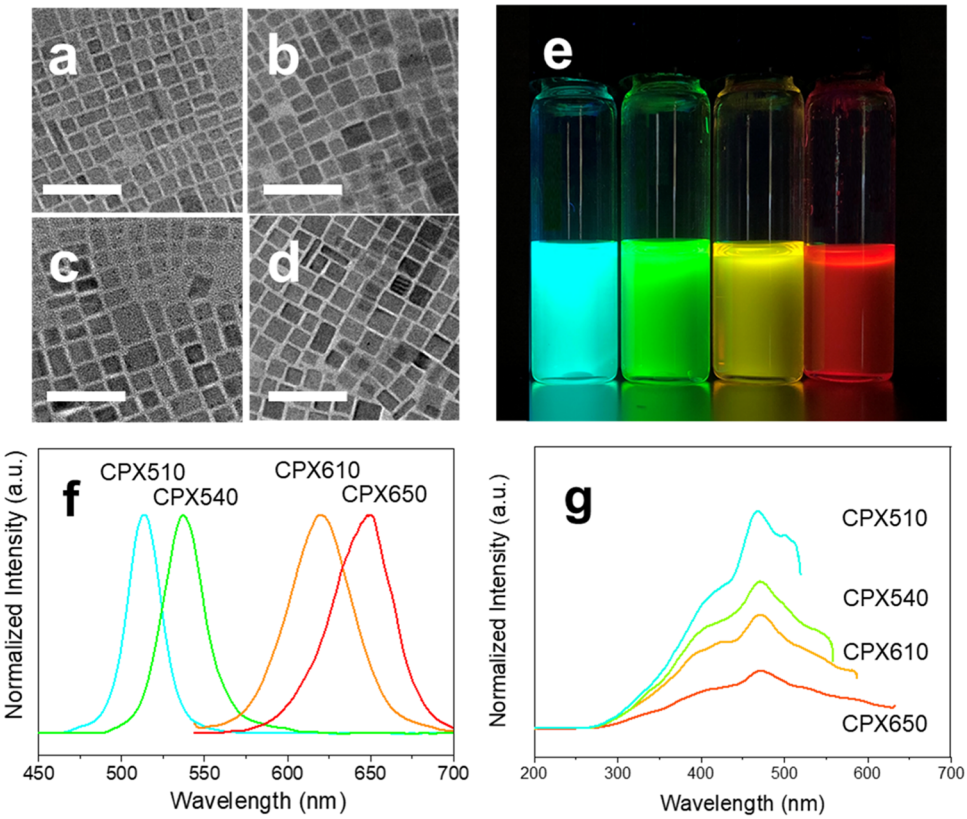

Figure 1. Physical characterization of cesium lead halide PeQDs used in the study. (a–d) TEM images of CPX510, CPX540, CPX610, and CPX650 samples, respectively. Scale bar: 50 nm. (e) Camera photo showing the luminescence color from different PeQD samples under 365 nm xenon light. (f) Emission spectra of different PeQD samples under 365 nm excitation and (g) corresponding excitation spectra.

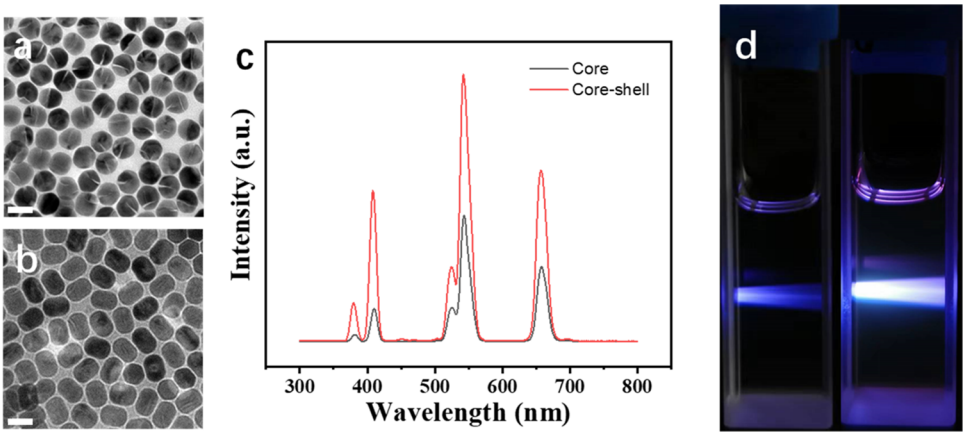

Figure 2. Physical characterization of UCNPs used in the study. (a, b) TEM images of $NaYF_4$:Yb,Tm cores and $NaYF_4$:Yb,Tm@$NaYF_4$ core–shell UCNPs, respectively. Scale bar: 50 nm. Upconversion spectra (c) and camera photos (d) of core and core–shell UCNP cyclohexane suspension under 980 nm NIR laser excitation.

further extended to other PeQDs, namely, CPX540, CPX610, and CPX650. Spectra showed that the same luminescence variation trends are observed for all PeQDs, with different single-peak emission profiles obtained based on the PeQDs used in the experiments (Figures S1–S3).

Obviously, these results demonstrate that the coupling between UCNPs and PeQDs is efficient and universal; therefore, we move on to tune the emission profiles of PeQDs after coupling with UCNPs by varying the halide composition ratio. ZnI_2 toluene solution is used as the halide exchange reagent to manipulate the UCL profiles of UCNP–PeQD pairs. ZnI_2 solution is obtained by dissolving 50 mg of ZnI_2 in 20 mL of toluene solution under sonication and vigorous stirring. A total of 100 μL of the as-prepared CPX510 cyclohexane suspension is mixed with different amounts of ZnI_2 toluene solution; the overall volume of the solution is topped up and kept the same at 1 mL throughout the experiment. The color of the mixture quickly changes right after the ZnI_2 toluene solution is added. Under 980 nm excitation, the emission peaks of the mixture are gradually red-shifted as the amount of the ZnI_2 toluene solution increased (Figure 4a). When 500 μL of the as-prepared ZnI_2 toluene

https://doi.org/10.1021/acsomega.2c06464
ACS Omega 2022, 7, 40596–40602

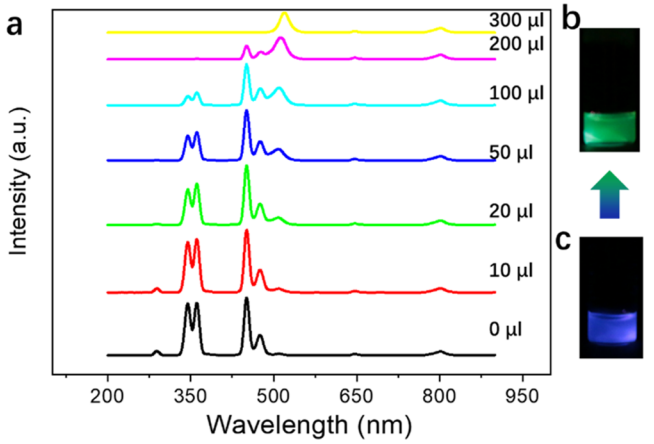

Figure 3. PeQD-modulated upconversion spectra. (a) UCL spectra of a 100 μL $NaYF_4$:30%Yb,0.5%Tm@$NaYF_4$ core−shell UCNP cyclohexane suspension mixed with different amounts of CPX510 samples. The added CPX510 suspension volume is specified alongside the curve, with the overall volume fixed at 1 mL. (b) Intrinsic and (c) CPX510-modulated UCL color under 980 nm excitation.

solution is added, the emission peak maximum is shifted to 650 nm. In addition, the emission of $NaYF_4$:30%Yb,0.5%Tm@$NaYF_4$ UCNPs still lies in the excitation profiles of PeQDs, indicating that the coupling between PeQDs and UCNPs is not affected by the halide exchange process (Figure 4b). To visualize the color shifting processes, the above-mentioned solutions are also patterned by stamping and dried under room temperature; under a 980 nm NIR laser, colors of the letters are red-shifted with increasing amount of ZnI_2 added (Figure 4c).

3.3. Double-Encrypted Strategy Using ZnI_2 as the Secret Ink. *3.3.1. Pattern Design and Printing.* As ZnI_2 can effectively manipulate the final UCL from UCNP−PeQD pairs, the encryption and anticounterfeiting potential of ZnI_2 and UCNP−PeQD pairs is explored and demonstrated. Briefly, UCNPs and ZnI_2 toluene solutions are used as a secret ink, while the double-encrypted information (the cut-away apple) is printed using ZnI_2 (Figure 5a). To make sure that the boundary is distinguishable and the patterning processes are repeatable, a commercialized inkjet printer (Cannon MG3100) is used to print the hidden pattern on a blank A4 paper. A ligand-free UCNP aqueous suspension and ZnI_2 solution are used as the ink and have been added in the cartridge before the printing tasks begin. The double-encrypted printing experiments begin with printing the UCNP suspension on a blank A4 paper; after it is completely dried, the ZnI_2 pattern is printed subsequently on the same A4 paper. To make sure that enough ZnI_2 is printed on the paper for the subsequent anion exchange, the ZnI_2 pattern is printed thrice. Notably, the A4 paper has to be completely dried after each printing job. Also, to make sure that the pattern is well collated, the paper needs to be well aligned before sending into the printer. To decrypt the hidden pattern, after the A4 paper is completely dried, a thin layer of CPX510 toluene solution as the decrypting reagent is evenly applied on top via brushing, and the paper is sent under the NIR animal-imaging system with 980 nm laser illumination to reveal the hidden pattern. As the control, in single-encryption design, only the UCNP suspension is printed on an A4 paper and the other steps are the same.

3.3.2. Decryption. Under 980 nm laser exposure, a hidden apple pattern in green color can be detected from both the double-encrypted A4 paper (with the hidden ZnI_2 pattern) and single-encrypted A4 paper (without the hidden ZnI_2 pattern) (Figure 5a,b). Note that the real-color figures are taken through a smartphone camera with a filter (blocking out the 980 nm laser signal), which made the camera go slightly out of focus; however, the boundary is clearly visible and sharp under a CCD camera (550/40) (Figure 5c,d). Notably, green rather than purple color is observed from the pattern, indicating that luminescence from UCNPs is fully absorbed and modulated by PeQDs. As the areas α and β are all decorated with UCNPs, under 980 nm NIR laser shining, the UV and blue emissions from UCNPs will illuminate all the PeQDs, giving off a full apple image; because the ZnI_2 pattern is printed first with a relatively small amount, the hidden information is covered at the bottom and not distinguishable. Therefore, if only a 980 nm laser is applied without choosing the right decoding channel, the secondary encrypted information is not decrypted. However, the emissive profile of the bottom PeQD layer applied on this region is red-shifted, and the hidden information can be detected in a longer wavelength range, i.e., using the decryption channel. When the imaging channel was switched to the decryption channel (660/50), a new pattern showing a cut-away apple is clearly observed because only the luminescence from area α, which contains the PeQDs that are modified with ZnI_2, can pass through the filter, while no hidden pattern is observed for the single-encryption group

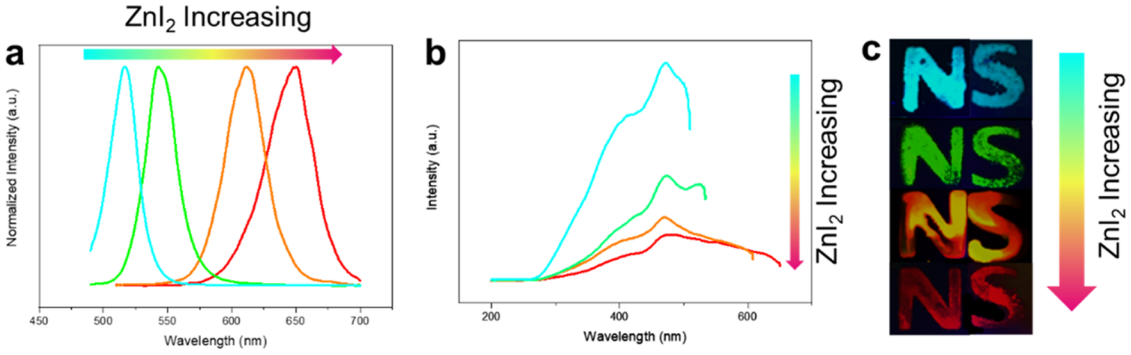

Figure 4. Tuning PeQD-modulated UCL via ZnI_2. (a) Normalized emission spectra and (b) excitation spectra of a 1 mL CPB510 cyclohexane suspension added with different amounts of ZnI_2 excited with 365 nm xenon light. (c) Revealing the upconversion luminescence pattern by shining the pattern with a 980 nm laser; patterns are created by stamping the above-mentioned PeQD and UCNP mixture added with different amounts of ZnI_2 on a paper.

https://doi.org/10.1021/acsomega.2c06464
ACS Omega 2022, 7, 40596−40602

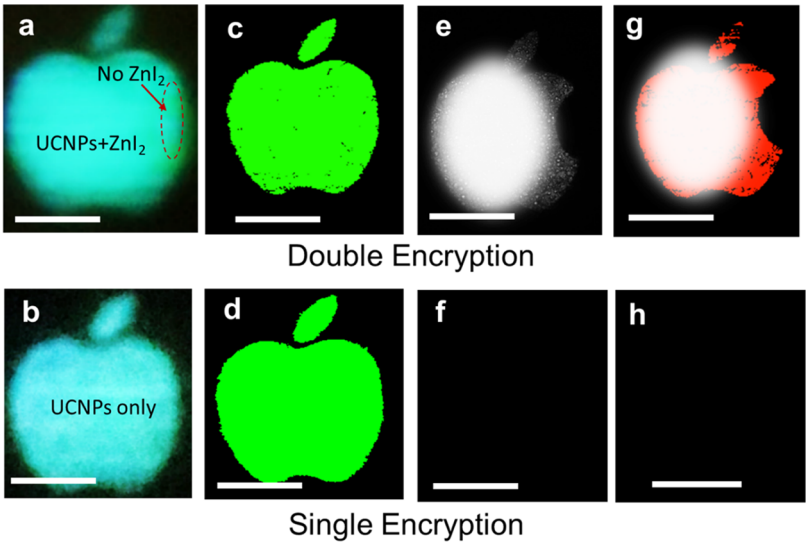

Figure 5. Inkjet printing of the double-encrypted anticounterfeiting pattern. (a, b) Camera photo and the layout of the anticounterfeiting pattern. (c, d) Pseudo-color image showing the hidden information under 980 nm excitation. (e–h) Camera photo and pseudo-color image showing the double-encrypted information under 980 nm excitation. Scale bar: 1 cm. Panels (e) and (g) are half-blurred to avoid the copyright issue.

due to the absence of the ZnI_2 pattern (Figure 5e–h). In addition, the pattern has been kept at room temperature for up to 24 h to study the stability of the pattern (Figure S6). Results show that the pattern can still maintain the distinguishable boundary and luminescence intensity for up to 10 min; after 1 h, the pattern gradually loses the boundary; due to the sensitivity of PeQDs to the environmental humidity, long-time exposure (24 h) in the atmosphere will lead to the luminescence quenching of PeQDs.

4. CONCLUSIONS

In this study, the coupling between $NaYF_4$:30%Yb,0.5%Tm@$NaYF_4$ UCNPs and different PeQDs is established. PeQDs render more luminescence possibility to UCNPs, while UCNPs provide PeQDs with anti-Stokes features, playing complementary roles to each other. Subsequently, ZnI_2 is introduced into the system to manipulate the UCL from the UCNP–PeQD pairs. Results show that the single-peak UCL profile of UCNP–PeQD pairs can be continuously shifted from green to red. Compared with varying the dopant concentration during the UCNP synthesis, our strategy offers great convenience and feasibility in UCL regulation, allowing the UCL emissive profile to be tuned after synthesis. Finally, a double-encrypted anticounterfeiting pattern is generated using an inkjet printer. The pattern encrypted information, which can only be decrypted under NIR laser excitation and a decryption channel. Notably, anion exchange and UCL regulation occur on the A4 paper; this in situ regulation strategy further expands the UCL manipulation possibility. The double-encryption strategy of using PeQDs, UCNPs, and ZnI_2 demonstrates anticounterfeiting potential in various fields such as confidential documents, industries, packaging, and so on. Moreover, the complementary roles of UCNPs and PeQDs to each other greatly expand the upconversion library, offering more feasibility in UCL regulation, and further promote practical applications in various fields such as displays, sensing, diagnostics, and so on.

■ ASSOCIATED CONTENT

Supporting Information

The Supporting Information is available free of charge at https://pubs.acs.org/doi/10.1021/acsomega.2c06464.

Material characterization and related spectrum data including the XRD characterization of UCNPs and PeQDs and UCL spectra of UCNP suspensions mixed with CPX540, CPX610, and CPX650 PeQDs (PDF)

■ AUTHOR INFORMATION

Corresponding Authors

Xiang Zheng − *Institute of Biomaterials and Tissue Engineering, Huaqiao University, Xiamen 361021, P. R. China; Fujian Provincial Key Laboratory of Biochemical Technology, Huaqiao University, Xiamen 361021, P. R. China;* orcid.org/0000-0002-8442-3339; Email: zhengxiang@hqu.edu.cn

Ai-Zheng Chen − *Institute of Biomaterials and Tissue Engineering, Huaqiao University, Xiamen 361021, P. R. China; Fujian Provincial Key Laboratory of Biochemical Technology, Huaqiao University, Xiamen 361021, P. R. China;* orcid.org/0000-0002-5840-3406; Email: azchen@hqu.edu.cn

Authors

Yuan Wen − *Institute of Biomaterials and Tissue Engineering, Huaqiao University, Xiamen 361021, P. R. China; Fujian Provincial Key Laboratory of Biochemical Technology, Huaqiao University, Xiamen 361021, P. R. China*

Jun Zhong − *Institute of Biomaterials and Tissue Engineering, Huaqiao University, Xiamen 361021, P. R. China; Fujian Provincial Key Laboratory of Biochemical Technology, Huaqiao University, Xiamen 361021, P. R. China*

Complete contact information is available at: https://pubs.acs.org/10.1021/acsomega.2c06464

Author Contributions

X.Z. conceptualized the project. A.-Z.C. funded the project. A.-Z.C. and X.Z. supervised the project. J.Z. and Y.W. completed

https://doi.org/10.1021/acsomega.2c06464
ACS Omega 2022, 7, 40596−40602

the main work of the experiment. X.Z. conducted the data analysis and wrote the original draft. J.Z. and Y.W. revised the article. All authors discussed the results and commented on the article.

Notes

The authors declare no competing financial interest.

■ ACKNOWLEDGMENTS

This work was financially supported by the Natural Science Foundation of Fujian Province (2020J01081), the National Key Research & Development Program of China (2019YFE0113600), the National Natural Science Foundation of China (NSFC, 81971734), and Program for Innovative Research Team in Science.

■ REFERENCES

(1) Qiao, T.; Son, D. H. Synthesis and Properties of Strongly Quantum-Confined Cesium Lead Halide Perovskite Nanocrystals. *Acc. Chem. Res.* **2021**, *54*, 1399−1408.

(2) Song, J.; Li, J.; Li, X.; Xu, L.; Dong, Y.; Zeng, H. Quantum Dot Light-Emitting Diodes Based on Inorganic Perovskite Cesium Lead Halides (CsPbX3). *Adv. Mater.* **2015**, *27*, 7162−7167.

(3) Hazarika, A.; Zhao, Q.; Gaulding, E. A.; Christians, J. A.; Dou, B.; Marshall, A. R.; Moot, T.; Berry, J. J.; Johnson, J. C.; Luther, J. M. Perovskite Quantum Dot Photovoltaic Materials beyond the Reach of Thin Films: Full-Range Tuning of A-Site Cation Composition. *ACS Nano* **2018**, *12*, 10327−10337.

(4) Jagadeeswararao, M.; Vashishtha, P.; Hooper, T. J. N.; Kanwat, A.; Lim, J. W. M.; Vishwanath, S. K.; Yantara, N.; Park, T.; Sum, T. C.; Chung, D. S.; Mhaisalkar, S. G.; Mathews, N. One-Pot Synthesis and Structural Evolution of Colloidal Cesium Lead Halide-Lead Sulfide Heterostructure Nanocrystals for Optoelectronic Applications. *J. Phys. Chem. Lett.* **2021**, *12*, 9569−9578.

(5) Shi, J.; Li, F.; Jin, Y.; Liu, C.; Cohen-Kleinstein, B.; Yuan, S.; Li, Y.; Wang, Z. K.; Yuan, J.; Ma, W. In Situ Ligand Bonding Management of CsPbI3 Perovskite Quantum Dots Enables High-Performance Photovoltaics and Red Light-Emitting Diodes. *Angew. Chem., Int. Ed.* **2020**, *59*, 22230−22237.

(6) Kim, J.; Seo, K. W.; Lee, S.; Kim, K.; Kim, C.; Lee, J. Y. All-in-One Process for Color Tuning and Patterning of Perovskite Quantum Dot Light-Emitting Diodes. *Adv. Sci.* **2022**, *9*, No. 2200073.

(7) Li, Y.; Zhang, X.; Huang, H.; Kershaw, S. V.; Rogach, A. L. Advances in metal halide perovskite nanocrystals: Synthetic strategies, growth mechanisms, and optoelectronic applications. *Mater. Today* **2020**, *32*, 204−221.

(8) Wang, J.; Chen, N.; Wang, W.; Li, Z.; Huang, B.; Yang, Y.; Yuan, Q. Room-Temperature Persistent Luminescence in Metal Halide Perovskite Nanocrystals for Solar-Driven CO_2 Bioreduction. *CCS Chem.* **2022**, 1.

(9) Huang, J.; Yan, L.; Liu, S.; Tao, L.; Zhou, B. Expanding the toolbox of photon upconversion for emerging frontier applications. *Mater. Horiz.* **2022**, *9*, 1167−1195.

(10) Lin, G.; Jin, D. Responsive Sensors of Upconversion Nanoparticles. *ACS Sens.* **2021**, *6*, 4272−4282.

(11) Sun, C.; Gradzielski, M. Advances in fluorescence sensing enabled by lanthanide-doped upconversion nanophosphors. *Adv. Colloid Interface Sci.* **2022**, *300*, No. 102579.

(12) Yuan, S.; Wang, J.; Xiang, Y.; Zheng, S.; Wu, Y.; Liu, J.; Zhu, X.; Zhang, Y. Shedding Light on Luminescent Janus Nanoparticles: From Synthesis to Photoluminescence and Applications. *Small* **2022**, *18*, No. 2200020.

(13) Li, Z.; Gao, H.; Shen, R.; Zhang, C.; Li, L.; Lv, Y.; Tang, L.; Du, Y.; Yuan, Q. Facet Selectivity Guided Assembly of Nanoarchitectures onto Two-Dimensional Metal−Organic Framework Nanosheets. *Angew. Chem., Int. Ed.* **2021**, *60*, 17564−17569.

(14) Yang, D.; Zou, Y.; Li, P.; Liu, Q.; Wu, L.; Hu, H.; Xu, Y.; Sun, B.; Zhang, Q.; Lee, S.-T. Large-scale synthesis of ultrathin cesium lead bromide perovskite nanoplates with precisely tunable dimensions and their application in blue light-emitting diodes. *Nano Energy* **2018**, *47*, 235−242.

(15) Ruan, L.; Zhang, Y. NIR-excitable heterostructured upconversion perovskite nanodots with improved stability. *Nat. Commun.* **2021**, *12*, No. 219.

(16) Zheng, W.; Huang, P.; Gong, Z.; Tu, D.; Xu, J.; Zou, Q.; Li, R.; You, W.; Bunzli, J. G.; Chen, X. Near-infrared-triggered photon upconversion tuning in all-inorganic cesium lead halide perovskite quantum dots. *Nat. Commun.* **2018**, *9*, No. 3462.

(17) Du, K.; Zhang, M.; Li, Y.; Li, H.; Liu, K.; Li, C.; Feng, J.; Zhang, H. Embellishment of Upconversion Nanoparticles with Ultrasmall Perovskite Quantum Dots for Full-Color Tunable, Dual-Modal Luminescence Anticounterfeiting. *Adv. Opt. Mater.* **2021**, *9*, No. 2100814.

(18) Gupta, A.; Ghosh, S.; Thakur, M. K.; Zhou, J.; Ostrikov, K.; Jin, D.; Chattopadhyay, S. Up-conversion hybrid nanomaterials for light- and heat-driven applications. *Prog. Mater. Sci.* **2021**, *121*, No. 100838.

(19) Sun, J.; Yang, X.; Sun, S.; Zhao, L.; Wang, S.; Li, Y. Recent progress of rare earth conversion material in perovskite solar cells: A mini review. *Inorg. Chem. Commun.* **2022**, *143*, No. 109731.

(20) Yang, B.; Wang, Y.; Wei, T.; Pan, Y.; Zhou, E.; Yuan, Z.; Han, Y.; Li, M.; Ling, X.; Yin, L.; Xie, X.; Huang, L. Solution-Processable Near-Infrared−Responsive Composite of Perovskite Nanowires and Photon-Upconversion Nanoparticles. *Adv. Funct. Mater.* **2018**, *28*, No. 1801782.

(21) Zheng, X.; Shikha, S.; Zhang, Y. Elimination of concentration dependent luminescence quenching in surface protected upconversion nanoparticles. *Nanoscale* **2018**, *10*, 16447−16454.

https://doi.org/10.1021/acsomega.2c06464
ACS Omega 2022, 7, 40596−40602